Journal of The Electrochemical Society, **161** (12) A1806-A1811 (2014)
0013-4651/2014/161(12)/A1806/6/$31.00 © The Electrochemical Society

Biocarbon Monoliths as Supercapacitor Electrodes: Influence of Wood Anisotropy on Their Electrical and Electrochemical Properties

Andrés Cuña,[a,b] Nestor Tancredi,[a,b,z] Juan Bussi,[a] Violeta Barranco,[c] Teresa A. Centeno,[d] Angie Quevedo,[a] and José M. Rojo[c]

[a]*Cátedra de Fisicoquímica, Laboratorio de Fisicoquímica de Superficies, DETEMA, Facultad de Química, Universidad de la República, Montevideo 11800, Uruguay*
[b]*Area Energías Renovables, Instituto Polo Tecnológico de Pando, Facultad de Química, Universidad de la República, Pando, Canelones 91000, Uruguay*
[c]*Instituto de Ciencia de Materiales de Madrid (ICMM), Consejo Superior de Investigaciones Científicas (CSIC), Cantoblanco 28049 Madrid, Spain*
[d]*Instituto Nacional del Carbón-CSIC, Oviedo 33080, Spain*

Biocarbon monoliths were obtained from *Eucalyptus grandis* and the influence of wood anisotropy on the electrical and electrochemical performance as supercapacitor electrodes was studied. They were produced from wood pieces cut along the transversal and longitudinal direction of the tree trunk, followed by pyrolysis and, for some of them, also by activation with CO_2. Monoliths with drilled channels were also obtained. All the monoliths were characterized by SEM, nitrogen adsorption/desorption isotherms, electrical conductivity measurements and electrochemical measurements, the latter in 2M aqueous H_2SO_4 electrolyte. Electrical conductivity and specific capacitance are higher for the transversal carbon monoliths than for the longitudinal ones. The electrical conductivity reaches values up to 27 S cm^{-1} for the transversal monolith. The specific capacitance reaches values up to 260 F g^{-1} for the transversal monolith that was activated and drilled. However, the highest volumetric capacitance, of 90 F cm^{-3}, is found for the longitudinal monolith that was activated and non-drilled. The energy density and power density, both referred to gravimetric and volumetric magnitudes, reach values as high as 36 Wh kg^{-1} and 12 Wh L^{-1}, and 2181 W kg^{-1} and 783 W L^{-1}, respectively. Comparison with a commercial powder activated carbon is provided.
 [DOI: 10.1149/2.0391412jes]

Manuscript submitted April 24, 2014; revised manuscript received August 7, 2014. Published August 21, 2014.

Supercapacitors are promising energy storage devices that bridge the gap between current conventional capacitors and batteries, offering higher energy density than conventional capacitors and higher power density and longer cycle life than batteries. They have found considerable interest in electric transportation technologies, emergency backup power and grid system stability and fuel cells.[1–3] Supercapacitor charge-discharge performs through the reversible electroadsorption and electrodesorption of the electrolyte ions at the surface of the active electrode material (double layer capacitance) as well as through reversible redox reactions (pseudocapacitance) in which are involved functional groups placed at the surface of the active electrode materials and some electrolyte ions. The three types of active electrode materials are: carbons, transition metal oxides and conducting polymers.

Carbon materials have been largely investigated as they meet all requirements for supercapacitor electrodes:[3–8] large specific surface area, open porosity, high conductivity, good electrochemical stability and moderate cost. Carbons are currently prepared from a wide variety of precursors, such as polymers, coals, biomass residues, etc.[9] Regarding the latter, they are a renewable source, available in large amounts, and still at low cost.[10–12] Their use as active electrode materials for supercapacitors has been already reported.[10,13–17]

Typical electrodes processed from a carbon powder as active electrode material usually requires the addition of: (i) a binder to conform the electrode, and (ii) a high electrical conductor to enhance the electrode electrical conductivity. However, the presence of the binder can hinder the access of the electrolyte to the pores of the active electrode material. If some particles of the active electrode material are embedded in the binder, they do not contribute to the electrode capacitance.[18–20]

Carbon monoliths are made from linked carbon particles and usually do not contain binders or other additives. They have been checked as supercapacitor electrodes and showed higher electrical conductivity, higher specific capacitance and better structural integrity than those items processed with binders.[20] In some monoliths, the presence of straight channels accounts for a rapid ionic transport between the electrolyte bulk and the carbon walls which leads to an enhanced capacitance retention at high current density.[21] Carbon monoliths are prepared from various precursors and by using different procedures: silica monoliths acting as templates,[22] fiberboard,[23] biomass materials,[24–26] mesophase pitch,[27] various synthetic polymeric materials,[28–32] bones,[33] etc. Recently, a surface-modified porous wood carbon monolith with high consistency and large porosity exhibited excellent electrochemical performance as compared with conventional electrodes made from activated carbon powder.[34] It is well-known that wood is an anisotropic raw material due to both cellular morphology and sub-cellular structural features; moreover, the carbon monoliths retain the anatomical characteristics of the precursor and their physical properties (mechanical properties, acoustic velocity, gas permeability) are directionally dependent.[26] However, in spite of the potentiality of the wood-based carbon electrodes, no studies dealing with the influence of the wood anisotropy on the electrical and electrochemical properties of the carbon monoliths have been carried out yet.

In this work, biocarbon monoliths are prepared from *E.grandis* wood pieces by pyrolysis and subsequent activation in CO_2. Wood pieces were cut in two directions, along the longitudinal and transversal direction of the tree trunk. In some particular cases, the wood pieces were also drilled to obtain channels in the carbon monolith. The performance of all carbon monoliths as electrodes for supercapacitors is studied and interpreted in relation to the two directions mentioned.

Experimental

Sample preparation.— Parallelepiped wood monoliths (WMs) were obtained from cutting pieces of *Eucalyptus grandis* wood along two directions. A convention for labeling the transversal and longitudinal cut directions of the wood is shown in Figure 1. In some particular cases, nine cylindrical straight channels of 1.5 mm in diameter were obtained by drilling normally to the WM largest rectangular face, with a Pro'skit PK-500 mini drill (Figure 2). Biocarbon monoliths (BCMs) were obtained by pyrolysis of WMs at 900 °C for 2 h under N_2 (99.998%) flow (200 mL min^{-1}). The heating rate was 2 °C min^{-1}. The cooling rate was uncontrolled to reach the room

[z]E-mail: nestor@fq.edu.uy

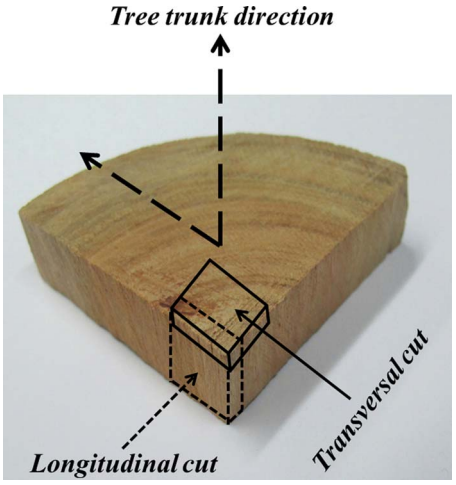

Figure 1. Convention for labeling the directions of transversal and longitudinal wood monoliths. The direction of the electric field for the electrochemical measurements is shown.

temperature. Other biocarbon monoliths (*a*BCMs) were obtained by activation of BCMs under CO_2 flow (200 mL min^{-1}) at 800 °C for 2 h. Under N_2 flow (200 mL min^{-1}), the temperature was risen up to 800 °C at 2 °C min^{-1}. Then the gas was changed to CO_2 keeping the same flow and the same temperature for 2 h. Once the time was over, the CO_2 flow was changed again to N_2, and the oven was switched off. All the thermal treatments were carried out in a horizontal Carbolite (CTF 12/75) oven. To label the monoliths, **T** and **L** stand for transversal and longitudinal cuts, respectively, ***a*** stands for the activated monoliths and ***d*** stands for the presence of drills. For comparison, a commercial powder activated carbon Norit DLC super-30 (called here-after Super-30) was chosen. Parallepiped pellets (10 mm × 3 mm × 2 mm) or cylindrical pellets (13 mm in diameter and 0.8 mm in height) were obtained by mixing and grinding the powder carbon with the powder polymer PVDF (10 wt%), and then by compacting at 2 Ton cm^{-2} for 2 min.

Scanning electron microscopy (SEM).— Pictures of the monoliths WMs, BCMs and *a*BCMs were obtained by a JEOL 5900 equipment.

Textural characterization.— The porous texture was studied by N_2 adsorption/desorption isotherms at 77 K, using a Micromeritics ASAP 2010. The analysis by the Dubinin-Radushkevich equation led to the volume of the micropores, W_0, the average micropore width, L_0, and the micropore surface area, S_{mic}. The external surface area, i.e. non-microporous, S_{ext}, and the total surface area, S_{comp} were deduced from comparison with a non-porous carbon used as reference (*Vulcan 3G*). A reliable value for the specific surface area (S_{av}) was calculated from the average of both determinations, $S_{av} = (S_{DR} + S_{comp})/2$, where $S_{DR} = S_{mic} + S_{ext}$.[35]

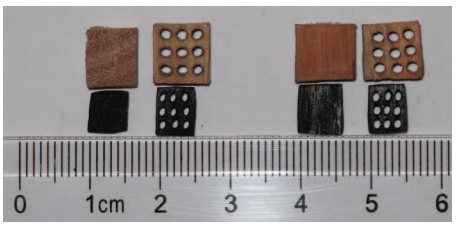

Figure 2. Representative photographs of the wood and biocarbon monoliths. Transversal monoliths and longitudinal ones are placed on the left and right hand of the figure.

Electrical conductivity measurements.— Electrical conductivity of the BCMs and *a*BCMs was measured by applying the electrical field in the direction perpendicular to the largest rectangular face by the four-probe Kelvin's method.[36] Then, the electrical measurements on the transversal monoliths were done along the direction of the tree trunk. The measurements on the longitudinal monoliths were done in a direction perpendicular to the tree trunk (Figure 1). The electrical measurements on the commercial activated carbon Super-30 were carried out on parallepiped pellets as already reported.[37] The four-probe AC measurements were carried out in a 1260 Solartron gain-phase analyzer (frequency range 0.1 Hz-1 MHz) at room temperature. A commercial silver paint was chosen to get the four probes. The electrical conductivity was determined according to $\sigma = l \cdot R^{-1} \cdot A^{-1}$; where R is the resistance measured, l is the distance between measuring voltage probes and A is the cross-section area.

Electrochemical measurements. Most measurements were carried out in two-electrode Swagelok™-type cells having two tantalum rods as current collectors. A glassy microfiber paper (Whatman 934 AH) was chosen as separator. The carbon monoliths had cross-section areas of 0.25–0.39 cm^2 and thicknesses of 0.12–0.25 cm. The weight of the monoliths was in the range 10–50 mg. The Super 30-based electrodes, of 60 mg in weight, had a cylindrical shape, of 13 mm in diameter and 0.8 mm in height. In all cases, the cross-section area was taken to determine the current density. 2M aqueous H_2SO_4 was the electrolyte. Before the cell assembly, the electrodes were soaked in the electrolyte under primary vacuum ($\approx 3 \cdot 10^3$ Pa). The specific (gravimetric) and volumetric capacitances were determined from galvanostatic charge/discharge measurements in the two-electrode cell. The specific capacitance C_s was determined according to the equation: $C_s = 2 \cdot I \cdot t_d/E_2 \cdot m_e$, where I is the current applied, t_d is the discharge time, E_2 is the voltage range during the discharge, and m_e is the mass of one carbon monolith, or the mass of Super-30 in one pellet. The volumetric capacitance C_V was determined according to the equation: $C_V = C_s \cdot \rho$, where ρ is the bulk density of the monoliths or the Super-30 pellet. The bulk density was determined by measuring the weight and the geometrical dimensions of each electrode either monolith or pellet. The voltage range was 0–1 V. The current densities applied were in the range 1–200 mA cm^{-2}.

In some particular cases, a three-electrode cell having the carbon monoliths as working electrodes, a platinum wire as counter electrode and Hg/Hg_2SO_4 as reference electrode was used. The electrolyte was the 2M aqueous solution H_2SO_4. For the two types of cells, the galvanostatic and voltammetric measurements were carried out at room temperature by a PGSTAT 302N Autolab potentiostat/galvanostat.

Results and Discussion

Morphological, textural and electrical characterization.— Figure 2 shows that the structural integrity of the wood monoliths (WM) is kept after pyrolysis and after pyrolysis plus activation. During the pyrolysis, the WM volume was reduced to about 60% for the transversal and longitudinal monoliths either undrilled or drilled. An additional shrinkage was observed after the subsequent CO_2 activation; it was higher for the transversal and drilled transversal monoliths (13.6%) than for the longitudinal and drilled longitudinal ones (1.3%). The activation degree (burn-off) was higher for the transversal monoliths (16 and 21% for T-*a*BCM and T-*a*BCM-*d*, respectively) than for the longitudinal ones (8 and 7% for L-*a*BCM and L-*a*BCM-*d*, respectively). Therefore, while the anisotropy of the wood monoliths does not induce any difference in the volume reduction during carbonization, that anisotropy makes easier the activation of the transversal monoliths as compared to the longitudinal ones. Probably the more open microstructure of the transversal carbon monolith (Figure 3c) favors its activation as compared to the longitudinal carbon monolith (Figure 3d). In any case, the same activation treatment leads to surface areas and micropore sizes that are different for the transversal and longitudinal activated monoliths, either drilled or not, as discussed below. Figures 3e and 3f on the one hand and Figures 4a and 4b on the other, clearly show that the microstructure of the activated carbon monoliths

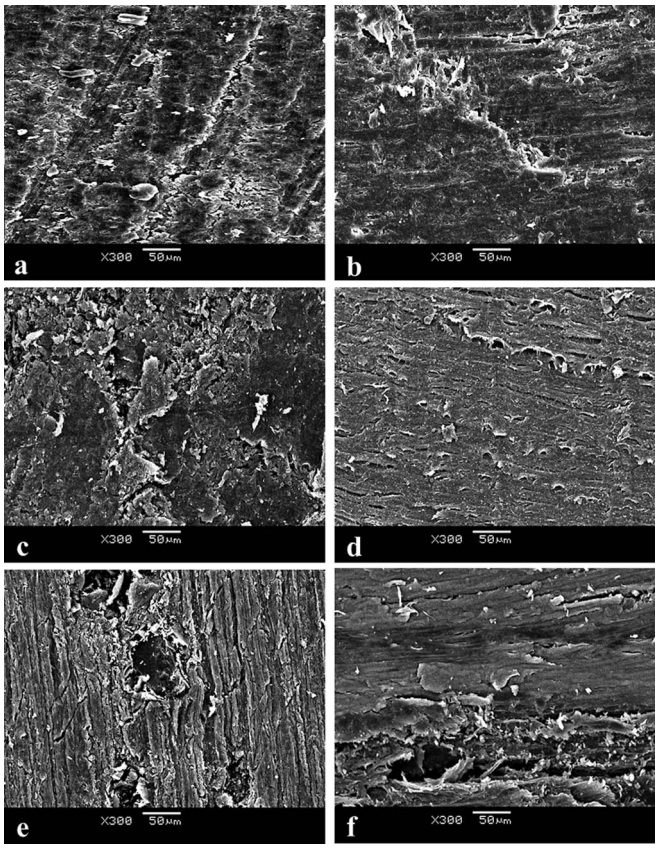

Figure 3. SEM micrographs of wood and biocarbon monoliths. (a) transversal wood monolith; b) longitudinal wood monolith; (c) transversal biocarbon monolith; (d) longitudinal bicarbon monolith; (e) transversal activated biocarbon monolith; (f) longitudinal activated bicarbon monolith. The pictures are taken on the largest rectangular face of the two types of monoliths.

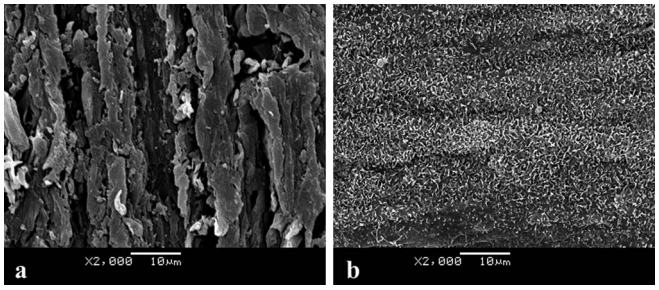

Figure 4. Magnified SEM pictures of the activated biocarbon monoliths. (a) transversal monolith; (b) longitudinal monolith. The pictures were taken on the largest rectangular face of the monoliths.

is more open for the transversal direction (along the tree trunk) than for the longitudinal direction (perpendicular to the tree trunk).

The textural parameters of all the carbon monoliths, transversal or longitudinal, activated or non-activated and drilled or undrilled, are summarized in Table I. With the exception of the longitudinal non-activated and undrilled monolith (L-BCM), all the other monoliths show porosity derived from the presence of micropores. The microporous surface area (S_{mic}) accounts for more than 92% of the total surface area (S_{av}). The transversal non-activated carbon monoliths, either undrilled (T-BCM) or drilled (T-BCM-*d*), show S_{av} values of 580 and 404 $m^2\ g^{-1}$, respectively. These values are higher than those corresponding to the longitudinal carbon monoliths, of 190 and 215 $m^2\ g^{-1}$ for L-BCM and L-BCM-*d*, respectively. Therefore, the same carbonization treatment leads to larger S_{av} for the transversal monoliths than for the longitudinal ones, i.e. S_{av} of the carbon monoliths depends on the anisotropy of the starting wood monoliths. According to the typical wood structure, elongated tubular cells and vessels are mainly aligned along the axis of the tree trunk;[26,38] this arrangement can favor the development of a larger S_{av} in the transversal carbon monoliths. Activation with CO_2 on the already obtained carbon monoliths leads to a significant increase of S_{av}. This parameter shows values of 917 and 923 $m^2\ g^{-1}$ for the transversal non-drilled monolith (T-*a*BCM) and drilled one (T-*a*BCM-*d*), respectively, and values of 587 and 679 for the longitudinal non-drilled monolith (L-*a*BCM) and drilled one (L-*a*BCM-*d*), respectively. The activated powder carbon Super-30 shows a value of S_{av} of 971 $m^2\ g^{-1}$, which is slightly higher than the values found for the transversal activated monoliths T-*a*BCM and T-*a*BCM-*d*. In relation to the average micropore size, the activation treatment does not change that parameter for the transversal monoliths but decreases that parameter for the longitudinal ones. Again, the development of porosity and surface area are affected by the anisotropy of the starting carbon monoliths. This result marks a difference from isotropic carbon monoliths obtained from chemical precursors. Regarding drilling on the two types of monoliths, either longitudinal or transversal, it does not appreciably change the average micropore size and the surface area, as deduced from Table I.

The electrical conductivity of the carbon monoliths is rather high, higher for the transversal monoliths than for the longitudinal ones and higher for the non-activated monoliths than for the activated ones (Table II). The higher values found for the transversal monoliths as compared to the longitudinal ones point out that the electrical conductivity is affected by the anisotropy of the monoliths. Moreover, the higher values found for the transversal monoliths point to a better connectivity of the carbon particles along the tree trunk direction. Other physical properties, such as the acoustic velocity, also displayed higher values along the tree trunk direction.[26] The activation treatment makes to decrease the electrical conductivity of the two kinds of carbon monoliths, longitudinal and transversal, as a consequence of the development of porosity; the decrease is higher than that reported for other isotropic carbon monoliths obtained from chemical precursors.[39] Comparing the activated carbon monoliths with the pellets having the activated carbon Super-30, the electrical conductivity of the former, either longitudinal or transversal, are at least one order of magnitude

Table I. Textural properties of transversal (T) and longitudinal (L) biocarbon monoliths (BCM), activated monoliths (*a*), and drilled (*d*) or not monoliths. The activated commercial Super-30 carbon is included as a reference.

Sample	V_{tot} ($cm^3\ g^{-1}$)	W_o ($cm^3\ g^{-1}$)	L_o (nm)	S_{mic} ($m^2\ g^{-1}$)	S_{ext} ($m^2\ g^{-1}$)	S_{tot} ($m^2\ g^{-1}$)	S_{comp} ($m^2\ g^{-1}$)	S_{av} ($m^2\ g^{-1}$)
T-BCM	0.17	0.17	0.61	557	2	559	600	580
T- BCM-*d*	0.16	0.16	0.78	413	1	414	394	404
T-*a*BCM	0.32	0.29	0.63	921	2	923	917	920
T-*a*BCM-*d*	0.45	0.37	0.81	914	9	923	923	923
L-BCM	0.12	0.09	>2	-	-	-	190	190
L-BCM-*d*	0.15	0.13	1.61	161	13	174	257	215
L-*a*BCM	0.30	0.25	0.95	526	63	589	584	587
L-*a*BCM-*d*	0.33	0.32	0.93	688	4	692	666	679
Super-30	0.79	0.60	1.24	968	9	977	965	971

Table II. Electrical conductivity (σ), specific (C_{S1}) and volumetric (C_{V1}) capacitance both measured at 1 mA cm^{-2}, and bulk density (ρ) of the biocarbon monoliths. T and L stand for transversal and longitudinal, respectively. *a* stands for activated monoliths. *d* stands for drilled monoliths. The results obtained for the activated commercial Super-30 carbon are taken as references.

Sample	σ (S cm^{-1})	C_{S1} (F g^{-1})	ρ (g cm^{-3})	C_{V1} (F cm^{-3})
T-BCM	27	50	0.36	18
T-BCM-*d*	-	47	0.30	14
T-*a*BCM	6	186	0.47	88
T-*a*BCM-*d*	-	260	0.34	88
L-BCM	17	37	0.59	22
L-BCM-*d*	-	55	0.52	28
L-*a*BCM	4	136	0.66	90
L-*a*BCM-*d*	-	180	0.40	73
Super-30	0.16	110	0.60	66

higher than the latter. It agrees with a better link of the carbon particles in the monolith than in the compacted pellet.[20]

Electrochemical characterization.— The galvanostatic plot obtained for the monolith T-*a*BCM-*d* in the two-electrode cell is shown as an example in Figure 5a. The discharge time (t_d) and the voltage range during discharge (E_2) are parameters measured at each current density to determine the specific and volumetric capacitance, energy and power. The dependence of the specific (gravimetric) and volumetric capacitance as a function of the current density is shown in Figures 5b and 5c, respectively. For all monoliths, and also for the compacted pellet having Super-30, C_S and C_V decrease as j increases. The decrease is associated with the presence of an equivalent series resistance (ESR) of the cells as usually observed. At low current density (1 mA cm^{-2}) our monoliths show values close to those reported for other carbon monoliths.[21,34,39,40] The activated monoliths, either transversal or longitudinal, show higher values of C_S and C_V than the corresponding non-activated monoliths. Moreover, the activated monoliths show higher values of C_S and C_V than the activated Super-30 carbon. The specific and volumetric capacitances measured at 1 mA cm^{-2} are compared for all the carbon monoliths as well as for Super-30 in Table II. Coming back to the Figures 5b and 5c, at higher current densities (i.e. > 1 mA cm^{-2}) the carbon monoliths prepared in this work show high capacitance retention, even higher than those reported in the literature. For instance, the carbon monolith T-*a*BCM-*d* shows a specific capacitance retention of 79% when j changes from 5 to 40 mA cm^{-2} while carbon monoliths obtained from poplar wood showed a capacitance retention of only 46% in the same range of j.[34]

Comparing the monoliths prepared in this work, it is observed that: (i) the non-activated carbon monoliths, either transversal or longitudinal, drilled or non-drilled, show low values of capacitances, below 60 F g^{-1} and 30 F cm^{-3} for C_{S1} and C_{V1}, respectively, (ii) the activated carbon monoliths show higher values of specific and volumetric capacitances as compared to the non-activated ones, (iii) the transversal activated monoliths show higher specific capacitances but similar volumetric capacitances than the longitudinal activated ones, and (iv) the drilled activated monoliths show higher specific capacitances but similar volumetric capacitances than the non-drilled activated ones. Therefore, the activation gives rise to an increase of the specific capacitance, the increase being more important for the transversal monoliths than for the longitudinal ones and for the drilled monoliths than for the undrilled ones. The activation also gives rise to an increase of the volumetric capacitance but the values of the volumetric capacitance are close for transversal and longitudinal, drilled and undrilled monoliths. This can be explained by the contribution of the bulk density to the volumetric capacitance, the density being lower for the transversal monoliths with regard to the longitudinal ones and for the drilled monoliths with regard to the undrilled ones (Table II).

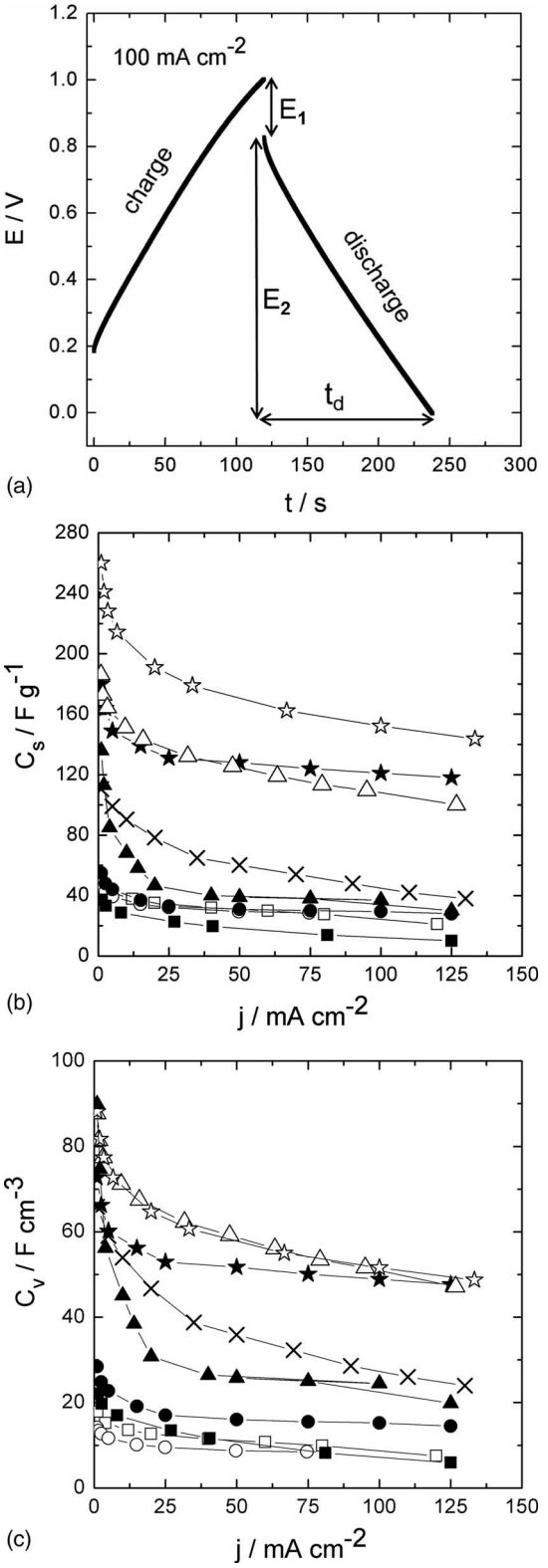

Figure 5. (a) Galvanostatic plot recorded on the monolith T-*a*BCM-*d* at the current density of 100 mA cm^{-2}. (b) Specific capacitance vs. current density for all monoliths and the activated commercial Super-30 carbon. Symbols stand for as follows: Open symbols for transversal monoliths and closed symbols for longitudinal monoliths. Stars for activated and drilled monoliths. Triangles for activated and undrilled monoliths. Circles for non-activated and drilled monoliths. Squares for non-activated and undrilled monoliths. Crosses for the activated commercial Super-30. (c) Volumetric capacitance vs. current density for all monoliths and the activated Super-30. Symbols stand for as in the caption of Figure 5b.

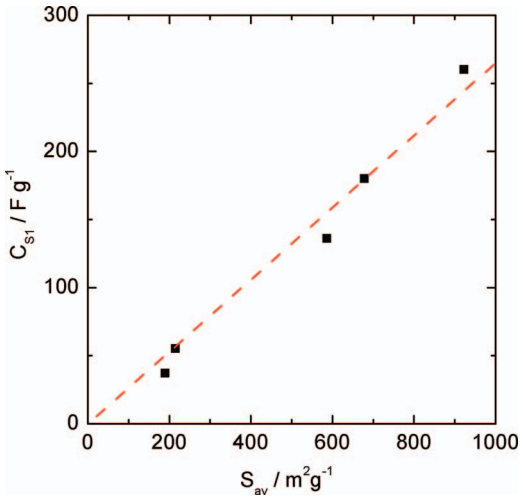

Figure 6. Dependence of the specific capacitance measured at 1 mA cm^{-2} as a function of the specific surface area. The straight line stands for the best fitting.

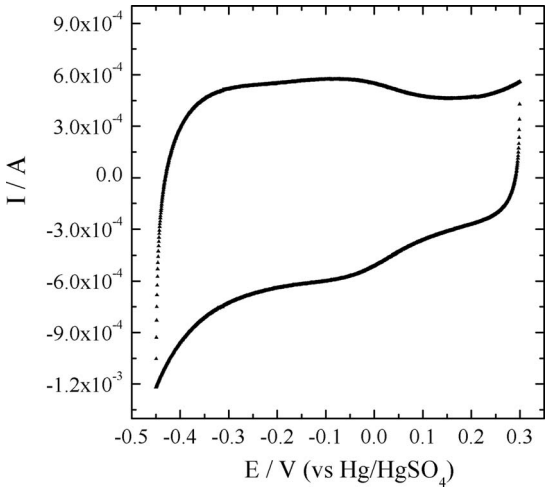

Figure 7. Cyclic voltammetry recorded on the monolith L-BCM-*d* at the scan rate of 0.5 mV s^{-1}. The measurements were carried out in a three-electrode cell in which Hg/Hg_2SO_4 was the reference electrode.

Assuming that the main contribution to the specific capacitance is due to the double layer capacitance, the specific capacitance measured at 1 mA cm^{-2} (C_{SI}), i.e. under conditions not affected by kinetic effects, can be discussed on the basis of the specific surface area (S_{av}) and the average micropore size (L_0). The plot of C_{S1} vs. S_{av} displaying scattered points (not shown) suggests that L_0 has some influence on the scattered pattern. An inspection of Table I show that not only S_{av} changes from monolith to monolith but L_0 changes as well. If L_0 shows a low value, the surface area due to micropores with sizes below L_0, i.e. due to the smaller micropores, could be not available to give the double layer with the electrolyte ions, and hence the double layer capacitance could be underestimated. It explains why the monoliths T-BCM, T-BCM-*d*, L-BCM and L-BCM-*d* show close values of C_{S1} while the two former monoliths show larger values of S_{av} as compared to the two latter ones. To check the effect of L_0 on C_{S1}, the monoliths having $L_0 < 0.8$ nm are ruled out and the plot of C_{S1} vs. S_{av} is shown in Figure 6. The linear dependence found, with a correlation factor of 0.998, accounts for proportionality between C_{S1} and S_{av}. The slope is 0.25 F m^{-2}. This value, which is much higher than that reported for a double layer capacitance, of ca. 0.10 F m^{-2} in acidic electrolyte,[35,41] evidences the presence of a significant pseudocapacitance. To check it, cyclic voltammetries were recorded in a three electrode cell for some carbon monoliths. Figure 7 shows as an example the humps observed at −0.05 and −0.3 V (vs Hg/Hg_2SO_4), which provide evidence of a pseudocapacitance in addition to the double layer capacitance.

The Ragone plots for the gravimetric and volumetric magnitudes are shown in Figures 8a and 8b, respectively. The gravimetric and volumetric energy densities W_S and W_V were calculated according to: $Ws = \frac{1}{2}\, C_S \cdot E_2^2$ and $W_V = \frac{1}{2}\, C_V \cdot E_2^2$, where C_S and C_V are the specific and volumetric capacitances measured at each current density and E_2 is the voltage range during the galvanostatic discharge at each current density (Figure 5a). The gravimetric and volumetric power densities P_S and P_V were calculated according to: $P_S = W_S/t_d$ and $P_V = W_V/t_d$, where t_d is the discharge time at each current density (Figure 5a). Comparing the carbon monoliths, the transversal monoliths (open symbols) show higher gravimetric energy and power density than the longitudinal ones (closed symbols). For the same type of carbon monolith, either longitudinal or transversal, the activated monoliths show higher gravimetric energy and power density than the starting ones. The drilled monoliths show better performances than the undrilled ones only on gravimetric energy and power density. Regarding the volumetric energy and power density, no significant differences are found for the longitudinal and transversal monoliths and for the drilled and undrilled monoliths. The activated monoliths show higher values in both volumetric energy and power density than

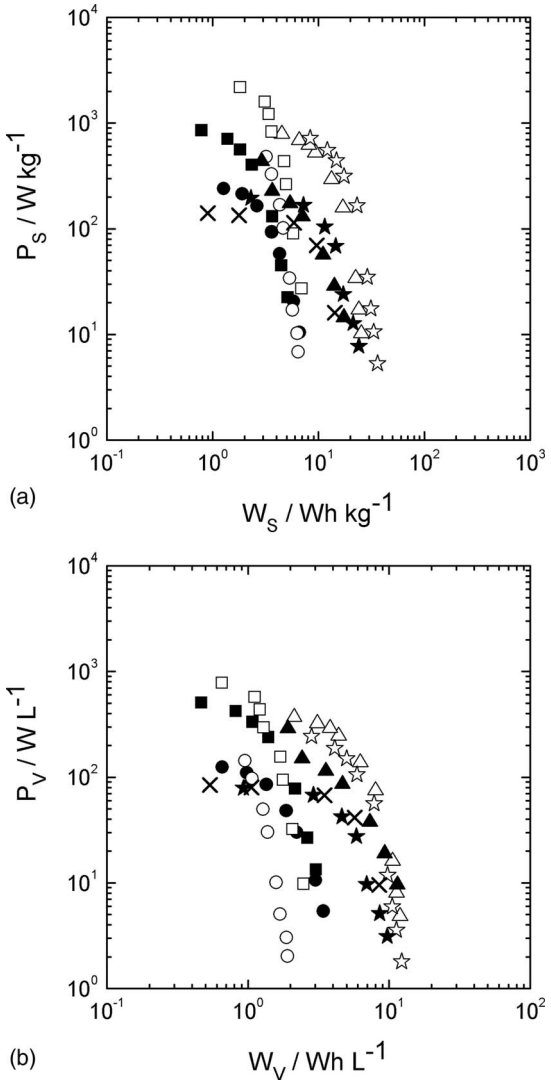

Figure 8. (a) Gravimetric power density vs. gravimetric energy density. (b) Volumetric power density vs. volumetric energy density. In (a) and (b) the symbols stand for as in the caption of Figure 5b.

the non-activated ones. The highest gravimetric energy density (Ws = 36 Wh kg^{-1}) and volumetric one (W_V = 12 Wh L^{-1}) is obtained for the monolith T-*a*BCM-*d*. The highest gravimetric power density (P_S = 2181 W kg^{-1}) and volumetric one (P_V = 783 W L^{-1}) is obtained for the monolith T-BCM. In comparison with the activated powder Super-30 carbon, the activated carbon monoliths have better performances, i.e. higher power density on both gravimetric and volumetric basis and higher energy density, manly on gravimetric basis.

Conclusions

Carbon monoliths were obtained by pyrolysis and by pyrolysis plus activation of pieces of *Eucalyptus grandis* wood, which were cut from two orientations: along and perpendicular to the tree trunk. The carbon monoliths are called longitudinal and transversal for the former and later orientation, respectively. After pyrolysis, the structural integrity of the wood monoliths is kept but the carbon monoliths are smaller than the wood monoliths. After activation with CO_2, the carbon monoliths shrink again, more for the transversal monoliths than for the longitudinal ones. Activation is favored on the transversal monoliths as deduced from the higher burn-off. The transversal carbon monoliths show larger surface areas and smaller micropores as compared to the longitudinal ones. The anisotropy of the carbon monoliths seems to come from the wood anisotropy.

The anisotropy marks differences in the electrical conductivity of the carbon monoliths. Transversal carbon monoliths show higher electrical conductivity than the longitudinal ones and the two types of monoliths show higher electrical conductivity than the compacted pellet made from commercial activated Super 30 carbon. In the two types of monoliths, the activation leads to a decrease of the electrical conductivity. The anisotropy marks also differences in the specific capacitance of the carbon monoliths, mainly for the activated monoliths. The transversal activated monoliths show higher specific capacitance than the longitudinal activated ones. Moreover, drilling leads to an improvement of the specific capacitance of the two types of activated monoliths, i.e. transversal and longitudinal. The volumetric capacitance is higher for the activated carbon monoliths than for the starting carbon ones; however there are not differences between the transversal and longitudinal monoliths and between the undrilled and drilled ones. The lack of differences on a volumetric basis comes from the contribution of the bulk density. The highest values of the electrical conductivity measured, up to 27 S cm^{-1}, specific capacitance, up to of 260 F g^{-1}, and volumetric capacitance, up to 90 F cm^{-3}, are comparable with the highest values reported for carbon monoliths obtained from chemical precursors. Those values are also higher than the values measured on a compacted pellet made from commercial activated Super-30 carbon.

Acknowledgments

Financial support from the projects (MAT 2011–25198, MP 1004 and ANII PR_FSE_2009_1_09) is gratefully acknowledged. A. Cuña thanks the Spanish AECID and Uruguayan ANII for the grants received. V. Barranco thanks the Spanish MINECO for R&C contract.

References

1. P. Sharma and T.S. Bhatti, *Energ. Convers. Manage.*, **51**, 2901 (2010).
2. P. Simon and Y. Gogotsi, *Nat. Mater.*, **7**, 845 (2008).
3. B. E. Conway, *Electrochemical Supercapacitors: Scientific Fundamentals and Technological Applications*, Kluwer Academic/Plenum Publishers, New York (1999).
4. M. Inagaki, H. Konno, and O. Tanaike, *J. Power Sources*, **195**, 7880 (2010).
5. A. G. Pandolfo and A. F. Hollenkamp, *J. Power Sources*, **157**, 11 (2006).
6. V. Barranco, V. Celorrio, M. J. Lázaro, and J. M. Rojo, *J. Electrochem. Soc.*, **159**, A464 (2012).
7. T. A Centeno, J. M. Hahn, J. Fernández, R. Kotz, and F. Stoeckli, *Electrochem. Commun.*, **9**, 1242 (2007).
8. E. Frackowiak and F. Béguin, *Carbon*, **39**, 937 (2001).
9. H. Marsh and F. Rodríguez-Reinoso, *Activated Carbon*, Elsevier, Oxford (2006).
10. T. E. Rufford, D. Hulicova-Jurcakova, Z. Zhu, and G. Q. Lu, *Electrochem. Commun.*, **10**, 1594 (2008).
11. O. Ioannidou and A. Zabaniotou, *Renew. Sust. Energ. Rev.*, **11**, 1966 (2007).
12. D. Savova, E. Apak, E. Ekinci, F. Yardim, N. Petrov, T. Budinova, M. Razvigorova, and V. Minkova, *Biomass Bioenerg.*, **21**,133 (2001).
13. C. Peng, X. Yan, R. Wang, J. Lang, Y. Ou, and Q. Xue, *Electrochim. Acta*, **87**, 401 (2013).
14. T. E. Rufford, D. Hulicova-Jurcakova, Z. Zhu, and G. Q. Lu, *J. Power Sources*, **195**, 912 (2010).
15. M. Biswal, A. Banerjee, M. Deo, and S. Ogale, *Energy Environ. Sci.*, **6**, 1249 (2013).
16. M. Olivares, J. A Fernández, J. M. Lázaro, C. Fernández, A. Macías, V. Gómez, F. Stoeckli, and T. A. Centeno, *Mater. Chem. Phys.*, **114**, 323 (2009).
17. G. Dobele, T. Dizhbite, M. V. Gil, A. Volpert, and T. A. Centeno, *Biomass Bioenerg.*, **46**, 145 (2012).
18. T. C. Weng and J. H. Teng, *J. Electrochem. Soc.*, **148**, A368 (2001).
19. J. Gamby, P. L. Taberna, P. Simon, J. F. Fauvarque, and M. Chesneau, *J. Power Sources*, **101**, 109 (2001).
20. A. Garcia, P. Miles, T. A. Centeno, and J. M. Rojo, *Electrochem. Solid-State Lett.*, **13**, A112 (2010).
21. A. García, P. Miles, T. A. Centeno, and J. M. Rojo, *Electrochimica Acta*, **55**, 8539 (2010).
22. O. Klepel, H. Strauß, A. Garsuch, and K. Böhme, *Mater. Lett.*, **61**, 2037 (2007).
23. A. K. Kercher and D. C. Nagle, *Carbon*, **41**, 3 (2003).
24. F. Kurosaki, H. Koyanaka, M. Tsujimoto, and Y. Imamura, *Carbon*, **46**, 850 (2008).
25. K. Laszlo, G. Onyestyak, C. Rochas, and E. Geissler, *Carbon*, **43**, 2402 (2005).
26. C. E. Byrne and D. C. Nagle, *Carbon*, **35**, 259 (1997).
27. P. Adelhelm, Y. S. Hu, L. Chuenchom, M. Antonietti, B. M. Smarsly, and J. Maier, *Adv. Mater.*, **19**, 4012 (2007).
28. S. Kang, J. S. Yu, M. Kruk, and M. Jaroniec, *Chem. Commun.*, **16**, 1670 (2002).
29. S. Han, K. Sohn, and T. Hyeon, *Chem. Mater.*, **12**, 3337 (2000).
30. Y. X. Wang, S. H. Tan, D. L. Jiang, and X. Y. Zhang, *Carbon*, **41**, 2065 (2003).
31. S. Alvarez, J. Esquena, C. Solans, and A. B. Fuertes, *Adv. Eng. Mater.*, **6**, 897 (2004).
32. K. Kanamori, K. Nakanishi, and T. Hanada, *Adv. Mater.*, **18**, 2407 (2006).
33. P. A. Goodman, H. Li, Y. Gao, Y. F. Lu, J. D. Stenger-Smith, and J. Redepenning, *Carbon*, **55**, 291 (2013).
34. M. C. Liu, L. B. Kong, P. Zhang, Y. C. Luo, and K. Long, *Electrochim. Acta*, **60**, 443 (2012).
35. F. Stoeckli and T. A. Centeno, *J. Mater. Chem.*, **A1**, 6865 (2013).
36. E. F. Northrup, *Methods of measuring electrical resistance*, McGraw-Hill Book Co, New York (1912).
37. A. Cuña, N. Tancredi, J. Bussi, A. C. Deiana, M. F. Sardella, V. Barranco, and J. M. Rojo, *Waste and Biomass. Valor.*, **5**(2), 305 (2014).
38. M. Lewin and I. Goldstein, *Wood structure and composition*, Marcel Dekker Inc, New York (1991).
39. M. Kunowsky, A. Garcia, V. Barranco, J. M. Rojo, J. Ibañez, D. Carruthers, and A. Linares-Solano, *Carbon*, **68**, 553 (2014).
40. V. Ruiz, C. Blanco, R. Santamaría, J. M. Ramos-Fernández, M. Martínez-Escandell, A. Sepúlveda-Escribano, and F. Rodríguez-Reinoso, *Carbon*, **47**, 195 (2009).
41. V. Barranco, M. A. Lillo-Rodenas, A. Linares-Solano, A. Oya, F. Pico, J. Ibañez, F. Agullo-Rueda, J. M. Amarilla, and J. M. Rojo, *J. Phys. Chem.*, **C 114**, 10302 (2010).